INTERNATIONAL JOURNAL FOR NUMERICAL AND ANALYTICAL METHODS IN GEOMECHANICS
Int. J. Numer. Anal. Meth. Geomech., 2007; **31**:933–952
Published online 26 October 2006 in Wiley InterScience (www.interscience.wiley.com). DOI: 10.1002/nag.569

On the mechanics of contact between a flexible transducer diaphragm located at a rigid boundary and an elastic material

A. P. S. Selvadurai*,†,‡, S. Labanieh and M. J. Boulon

Laboratoire Sols, Structures, Solides, Université Joseph Fourier, Grenoble, France

Dedicated to Professor R. E. Gibson, FREng, on the occasion of his 80th birthday.

SUMMARY

In this paper we examine the mechanics of contact between a flexible elastic diaphragm and an isotropic elastic halfspace region where contact is established through the application of a normal stress. It is shown that a convenient solution for the maximum displacement and maximum flexural moment in the flexible diaphragm can be obtained by employing a variational technique. Copyright © 2006 John Wiley & Sons, Ltd.

Received 18 July 2006; Accepted 11 September 2006

KEY WORDS: contact pressure transducer; sensor with flexible diaphragm; variational solution; elastic halfspace–plate interaction; mechanics of sensors; arching action in pressure

1. INTRODUCTION

Contact pressure sensors are devices that are used to determine the magnitude and distribution of stresses at the region of contact between material bodies. The applications of contact pressure sensors are numerous, ranging from tactile sensor-based robotic components used in manufacturing, control of materials handling during bulk flow of solids in industrial processes and packaging, biomedical applications involving prostheses, monitoring in geophysical, energy resources and environmental applications, and in civil and mechanical engineering applications for monitoring the performance of structures and components. The literature in this area is vast and no attempt will be made to provide a comprehensive review of the general area of contact pressure sensors in engineering. The reader is referred to the volumes by Hast [1], Hvorslev [2], Selvadurai [3], Kulhawy [4], Hanna [5], Dunnicliffe and Green [6], Sinha [7] and Lazebnik [8] on aspects of pressure sensors used in geomechanics. References [3, 8] in particular contain reviews of

*Correspondence to: A. P. S. Selvadurai, Laboratoire Sols, Structures, Solides, Université Joseph Fourier, Grenoble, France.
†E-mail: patrick.selvadurai@mcgill.ca
‡Permanent affiliation: William Scott Professor and James McGill Professor, Department of Civil Engineering and Applied Mechanics, McGill University, Montréal, QC, Canada H3A 2K6.

the application of pressure transducers in the measurement of contact pressures at soil–structural foundation interfaces and articles dealing with issues related to calibration of the cell-action under laboratory conditions. Other applications of contact stress measurement as applied to micro-electronic measuring systems, tactile sensors, elasto-hydrodynamics and prosthetic biomechanics are given, among others, by Webster [9], Tandeske [10], Bao [11], Mak *et al.* [12], Gohar [13], Gad-el-Hak [14], Boyes [15], Beeby [16], Nawrocki [17], Dunn [18] and Lewis [19, 20].

In this paper we examine a contact mechanics problem that is of interest to the modelling of the interaction between the flexible diaphragm of a pressure transducer, which maintains frictionless contact with an elastic body of semi-infinite extent. In the field of geomechanics, such contact pressure transducers are used quite extensively at the boundary of structural elements including foundations of dams and buildings and at the contact surfaces between earth retaining structures. The information derived from contact pressure measurements provides valuable information for examining the validity of constitutive theories of geomaterial behaviour and computational techniques for examining soil–structure interaction problems. The contact mechanics of the interaction between deformable bodies is influenced by the constitutive responses of the media in contact. In this sense, the interpretation of the measurements derived from a contact pressure transducer *cannot* be without a prior knowledge of these constitutive responses. Also, the sensing process usually involves the measurement of either the displacements or the strains of the active diaphragm region. The principle here is that 'what can be measured is what can be seen, which is a displacement, and the rest is interpretation'. The interpretation of the far-field pressure from the measurement of either the deflections or the strains in the diaphragm therefore requires assumptions related to the deformability characteristics of the diaphragm, the influence of contact friction and the constitutive response of the medium through which the far-field stresses are transmitted. The analysis of such a generalized problem invariably requires recourse to computational approaches. Experimental investigations involving the performance of boundary pressure cells in contact with geomaterials have been made by a number of investigators and these results are documented in the relevant references cited previously. An important observation in this regard is that the calibration of the pressure sensor is usually done through the application of a fluid (either air or water or oil) pressure to the surface of the diaphragm. These calibrations are therefore valid strictly in situations where the contacting medium is a fluid. Geomaterials on the other hand can possess a discrete internal fabric and/or a continuum structure along with complicated constitutive responses that can influence the load transfer within them. This leads to inconsistencies between the interpretation of pressures measured through transducers that are in contact with geomaterials. Figure 1 shows the results obtained by Labanieh and Elhajal [21] from an experimental investigation of the loading of a pressure transducer located at a rigid boundary and in contact with a granular medium. The pressure transducer was a KYOWA-type miniature pressure transducer of contact surface diameter 6 mm. The applied load was transmitted to the pressure transducer through a layer of fine sand of thickness 20 mm and diameter 100 mm. The test was conducted in an oedometric condition and the external pressure was applied to the surface of the sand layer through a rubber membrane of approximate thickness 0.5 mm. Figure 1 illustrates the variation in the applied pressure *vs* the pressure interpreted through the transducer response, for various densities of the granular material ranging from 1.42 to 1.66 g/cc. Figure 1 also provides the result for the case where the pressures are transmitted through water. As is evident, the pressures measured using the contact pressure transducer drastically underestimated the pressures that were applied to the surface of the sand

DOI: 10.1002/nag

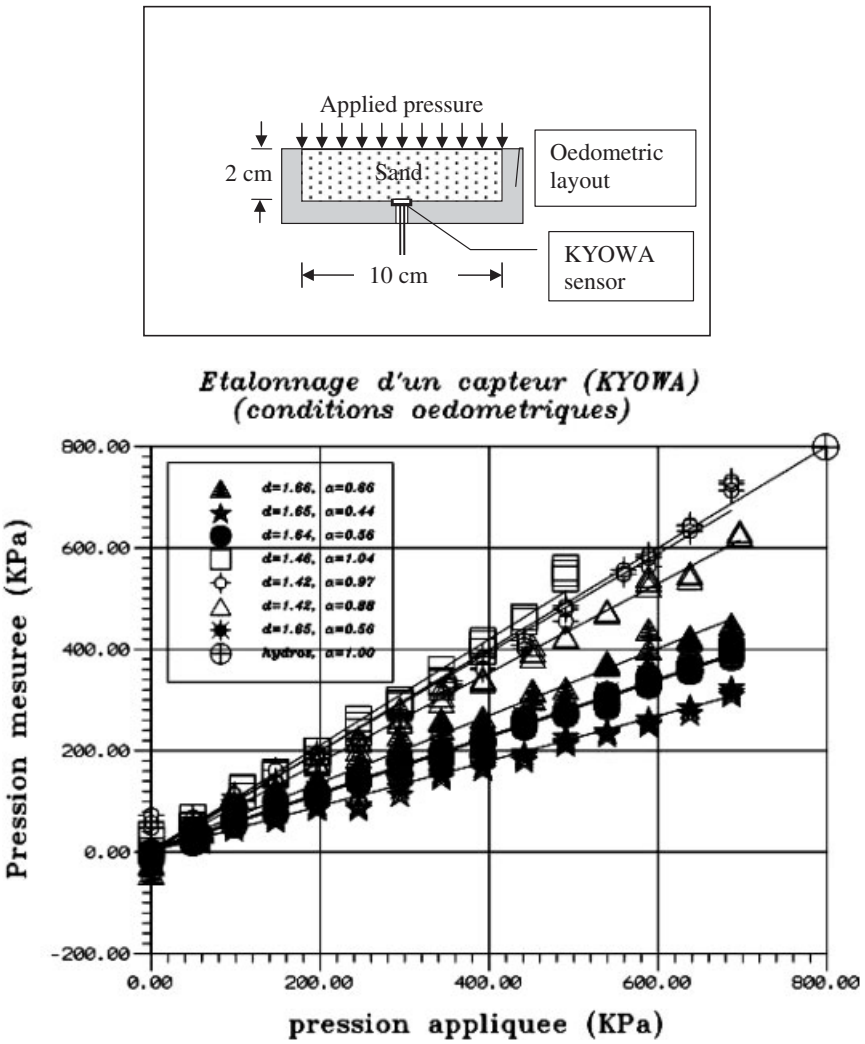

Figure 1. Correlation between an applied pressure and the pressure inferred from measurements made by a contact pressure transducer located at a rigid boundary (after Labanieh and Elhajal [21]).

layer. Although some frictional effects can be present along the cylindrical surface of the oedometer, the discrepancy of nearly 100% at high densities cannot be explained through the consideration of these frictional losses. The importance of the consideration of the action of a pressure cell as a boundary value problem is therefore clear. In order to interpret the data obtained from a pressure cell, either the cell must be calibrated in an environment identical to its intended use or a rational theoretical model of a cell–geomaterial interaction problem should be solved with a prior knowledge of the constitutive response of the geomaterial and the interacting components including contacting interfaces.

The objective of this paper is to consider a simplified problem that deals with the mechanics of frictionless contact between a flexible circular diaphragm and an elastic body, which is induced by

DOI: 10.1002/nag

a far-field normal stress. Under the action of the normal stress, the diaphragm can undergo axisymmetric flexure, which in turn influences the contact stress field and the associated deflections of the diaphragm. The resulting elasto-static contact problem is analysed using a variational approach consistent with a prescribed deflected shape of the elastic diaphragm. Selvadurai [22–24] has shown that a variational approach that utilizes the results of mixed boundary value problems in classical elasticity is a convenient and effective technique for the study of the interaction between an elastic halfspace and structural elements such as beams and plates. This paper applies the variational technique to develop an approximate solution to the title problem.

2. THE VARIATIONAL FORMULATION

We examine the problem of the axisymmetric interaction between a flexible elastic diaphragm of radius a that is located at a rigid boundary and an elastic medium of semi-infinite extent. Both the surface of the elastic diaphragm and the surface of the rigid boundary are assumed to be frictionless. The flexural interaction is induced by a far-field stress p_0 that acts normal to the plane of the rigid boundary (Figure 2). We assume that the flexural behaviour of the elastic diaphragm can be described by the classical Poisson–Kirchhoff–Germain thin plate theory [3, 25, 26] and, in accordance with the thin plate theory as well as the classical theory of elasticity, the deflections are assumed to be small in comparison to the thickness of the plate and the strains correspondingly smaller than unity. The complete formulation of the problem requires the solution of an integro-differential equation system for the deflection $w(r)$ of the diaphragm, characterized by the following: the deflection of the diaphragm is governed by

$$D\nabla^2\nabla^2 w(r) + q(r) = p_0 \tag{1}$$

where the contact pressure $q(r)$ is related to the deflection $w(r)$ through the integral equation

$$w(r) = \frac{(1-\nu)}{G}\int_0^a \int_0^{2\pi} \frac{q(\varsigma)\varsigma \, \mathrm{d}\varsigma \, \mathrm{d}\varphi}{[r^2 + \varsigma^2 - 2r\varsigma\cos\varphi]^{1/2}} \tag{2}$$

In (1) and (2), $D(= G_{\mathrm{p}}h^3/6(1-\nu_{\mathrm{p}}))$ is the flexural rigidity of the diaphragm; G_{p} and ν_{p} are, respectively, the linear elastic shear modulus and Poisson's ratio for the diaphragm material; h is the diaphragm thickness, and G and ν are the elastic constants for the contacting medium. The

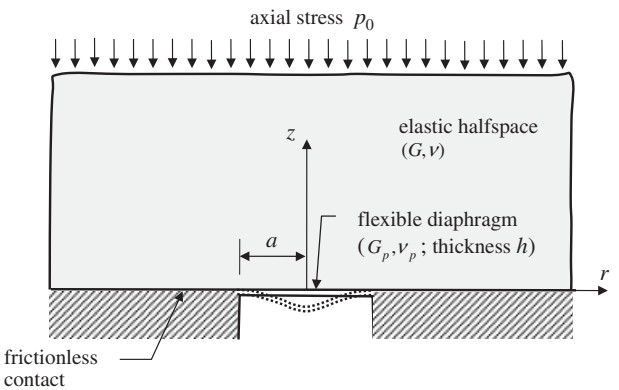

Figure 2. Geometry of the diaphragm for the contact problem. Deflected shape defined by (6).

DOI: 10.1002/nag

plate bending equation for the diaphragm is subject to the boundary conditions

$$[w(r)]_{r=a} = \left[\frac{\mathrm{d}w(r)}{\mathrm{d}r}\right]_{r=0} = \left[\frac{\mathrm{d}w(r)}{\mathrm{d}r}\right]_{r=a} = 0 \tag{3}$$

$$w(r) = 0, \quad r \in (a, \infty) \tag{4}$$

along with the consistency condition

$$\lim_{c\to\infty} \int_0^c [q(r) - p_0] r \, \mathrm{d}r = 0 \tag{5}$$

where c is any radius on the contact interface. The solution of the boundary value problem posed by (1)–(5), entails its reduction essentially to a Fredholm integral equation of the second kind for an unknown function, which can be solved only in a numerical fashion using either a series expansion technique, or a collocation technique or a variational technique. The approach adopted here is to consider a *direct variational treatment* of the interaction between the diaphragm and the elastic halfspace region, in which the deflection of the diaphragm is specified, to satisfy the *natural boundary conditions* applicable to a thin plate. In prescribing such a deflection field, it is necessary to consider the boundary conditions applicable to the edge of the diaphragm region. We assume that the deflections of the diaphragm will satisfy both the zero displacement and zero slope conditions at the boundary $r = a$. Furthermore, for kinematic admissibility, the slope of the deflected shape of the diaphragm should be zero at the location $r = 0$. We select a form of the plate deflection $w(r)$ defined by

$$w(r) = -\frac{C_0}{a^3}[a^2 - r^2]^2 \tag{6}$$

where C_0 is an undetermined multiplier and the deflection is assumed to occur in the direction indicated in Figure 2. This form of an expression for the deflection of the diaphragm will identically satisfy the kinematic constraints

$$w(a) = \left[\frac{\mathrm{d}w}{\mathrm{d}r}\right]_{r=0} = \left[\frac{\mathrm{d}w}{\mathrm{d}r}\right]_{r=a} = 0 \tag{7}$$

for any choice of the multiplier C_0. The requirement of zero slope for the deflected shape of the diaphragm at $r = a$, places a non-zero constraint on the stiffness of the diaphragm. The analysis can be extended to consider other forms of boundary conditions where the zero slope edge condition in (7) is relaxed; but the zero slope condition is considered to be a more realistic representation of the deflected profile of a transducer diaphragm that is expected to experience minimal deflection under the interaction. We further assume that during the application of the external stress p_0 the diaphragm will maintain complete frictionless contact with the elastic halfspace region.

We now focus attention on the variational formulation of the interaction between the diaphragm and the elastic halfspace region consistent with the assumed form of the diaphragm deflection (6). In order to develop the *total potential energy functional* for the problem we require that the contact pressures developed within the diaphragm region as it deflects maintain complete contact with the elastic halfspace region. In the case where the diaphragm does not deflect, the conditions of equilibrium and symmetry will dictate that the axial and shear stresses on the plane of the diaphragm will be given by

$$\sigma_{zz}(r, 0) = -p_0, \quad r \in (0, \infty) \tag{8}$$

DOI: 10.1002/nag

$$u_z(r,0) = 0, \quad r \in (0,\infty) \tag{9}$$

$$\sigma_{rz}(r,0) = 0, \quad r \in (0,\infty) \tag{10}$$

where σ_{ij} are the components of the Cauchy stress tensor referred to the cylindrical polar coordinate system. During the deflection of the diaphragm, the normal stresses acting within the diaphragm region $r \in (0,a)$ will change. In order to determine this change in the contact normal stress we examine the following mixed boundary value problem:

$$\sigma_{zz}(r,0) = p(r), \quad r \in (0,a) \tag{11}$$

$$u_z(r,0) = 0, \quad r \in (a,\infty) \tag{12}$$

$$\sigma_{rz}(r,0) = 0, \quad r \in (0,\infty) \tag{13}$$

where $p(r)$ can be identified with the tensile normal traction associated with the axial displacement

$$u_z(r,0) = w(r), \quad r \in (0,a) \tag{14}$$

In addition, the solution of the mixed boundary value problem posed by (11)–(13) should satisfy the regularity conditions, in that the displacement and stress fields reduce to zero as both $r, z \to \infty$, thereby maintaining the far-field stress state at the initially specified value of the compression p_0. The solution of the axisymmetric mixed boundary value problem posed by (11)–(13) is relatively routine and details of the procedures are given by Sneddon [27, 28], in connection with the solution of the penny-shaped crack problem for an isotropic elastic solid. Briefly, using a Hankel transform representation of the solution to the axisymmetric problem in the classical theory of elasticity formulated in terms of either the biharmonic strain potential of Love [26, 29] or the single harmonic function approach outlined by Green [30], the mixed boundary value problem can be effectively reduced to the solution of the pair of dual integral equations

$$\int_0^\infty \xi A(\xi) J_0(\xi r)\, \mathrm{d}\xi = \frac{p(r)}{2G}, \quad r \in (0,a) \tag{15}$$

$$\int_0^\infty A(\xi) J_0(\xi r)\, \mathrm{d}\xi = 0, \quad r \in (a,\infty) \tag{16}$$

for a single unknown function $A(\xi)$. In these equations $J_0(\xi r)$ is the zeroth-order Bessel function of the first kind and G is the linear elastic shear modulus. The solution of the dual system is given by Sneddon [27, 28] and it involves the reduction of the system to an Abel integral equation of the first kind through the use of a finite Fourier transform to satisfy Equation (16) explicitly. The result of importance to the diaphragm–elastic halfspace interaction problem relates to the displacement within the diaphragm region, which can be expressed in the form

$$u_z(r,0) = w(r) = \frac{(1-\nu)}{G} \int_r^a \frac{g(s)\, \mathrm{d}s}{\sqrt{s^2 - r^2}}, \quad r \in (0,a) \tag{17}$$

where

$$g(r) = \frac{2}{\pi} \int_0^r \frac{tp(t)\, \mathrm{d}t}{\sqrt{r^2 - t^2}} \tag{18}$$

DOI: 10.1002/nag

and v is Poisson's ratio for the elastic medium in contact with the diaphragm. The approach adopted here is to *successively invert* the Abel integral equations (17) and (18) to determine $p(r)$ corresponding to the prescribed axial displacement $w(r)$. Using the inversion relationships [28, 31] we can show that

$$g(r) = -\frac{2G}{\pi(1-v)}\frac{\mathrm{d}}{\mathrm{d}r}\int_r^a \frac{tw(t)\,\mathrm{d}t}{\sqrt{t^2-r^2}} \tag{19}$$

$$p(r) = \frac{1}{r}\frac{\mathrm{d}}{\mathrm{d}r}\int_0^r \frac{tg(t)\,\mathrm{d}t}{\sqrt{r^2-t^2}} \tag{20}$$

The tensile stress required to induce the displacement $w(r)$ (given by (6)) within the diaphragm region is

$$\sigma_{zz}(r,0) = p(r) = \frac{GC_0}{(1-v)}\left[\frac{8}{3}\,{}_2F_1\left(-\frac{3}{2},\frac{3}{2};2;\frac{r^2}{a^2}\right) - 3\left(\frac{r^2}{a^2}\right)\,{}_2F_1\left(-\frac{1}{2},\frac{5}{2};3;\frac{r^2}{a^2}\right)\right] \tag{21}$$

where ${}_2F_1(\tilde{a},b;c;z)$ is the Hypergeometric function [32], which has the series expansion

$${}_2F_1(\tilde{a},b;c;\zeta) = \sum_{k=0}^{\infty}\frac{(\tilde{a})_k(b)_k}{(c)_k}\frac{\zeta^k}{k!} \tag{22}$$

As the diaphragm deflects, strain energy is released from the elastic halfspace region initially constrained to maintain the boundary condition (9). This strain energy can be calculated by considering the work done by the tractions $p(r)$ associated with the displacement $w(r)$ i.e.

$$U_{\mathrm{HS}} = \frac{\pi GC_0^2}{(1-v)a^3}\int_0^a \left[\frac{8}{3}\,{}_2F_1\left(-\frac{3}{2},\frac{3}{2};2;\frac{r^2}{a^2}\right) - \left\{3\left(\frac{r^2}{a^2}\right)\,{}_2F_1\left(-\frac{1}{2},\frac{5}{2};3;\frac{r^2}{a^2}\right)\right\}\right] \times r(a^2-r^2)^2\,\mathrm{d}r \tag{23}$$

The integral in (23) can be evaluated in *exact closed form* giving

$$U_{\mathrm{HS}} = \frac{\kappa a^3 GC_0^2}{(1-v)} \tag{24}$$

where $\kappa(=2048/2835)$ is a constant. Flexural energy is stored in the diaphragm by virtue of its deflected shape. For axisymmetric deflections of the diaphragm, the flexural energy in the plate can be evaluated from the expression

$$U_{\mathrm{F}} = \pi D\int_0^a \left[(\nabla^2 w(r))^2 - \frac{2(1-v_{\mathrm{p}})}{r}\frac{\mathrm{d}w(r)}{\mathrm{d}r}\frac{\mathrm{d}^2 w(r)}{\mathrm{d}r^2}\right] r\,\mathrm{d}r = \frac{32\pi DC_0^2}{3} \tag{25}$$

The potential energy of the tractions p_0 originally acting within the active area of the flexible diaphragm is given by

$$U_{\mathrm{p}} = -2\pi p_0\int_0^a \frac{C_0}{a^3}(a^2-r^2)^2 r\,\mathrm{d}r = -\frac{\pi p_0 C_0 a^3}{3} \tag{26}$$

The total potential energy function for the elastic diaphragm–elastic medium system under the action of the far-field normal stress p_0 and consistent with the assumed deflected shape (6) is given by

$$U = \frac{\kappa a^3 GC_0^2}{(1-v)} + \frac{32\pi DC_0^2}{3} - \frac{\pi p_0 C_0 a^3}{3} \tag{27}$$

DOI: 10.1002/nag

For the total potential energy function for the system to be an extremum with respect to the kinematically admissible deflection specified by (6), we require

$$\frac{\partial U}{\partial C_0} = 0 \tag{28}$$

This procedure can be used to obtain the following expression for the deflection of the diaphragm:

$$w(r) = \frac{\pi p_0 a(1-\nu)}{G(6\kappa + \Omega\lambda_1)}\left(1 - \frac{r^2}{a^2}\right)^2 \tag{29}$$

where Ω is a relative stiffness parameter and λ_1 is a constant defined by

$$\Omega = \frac{G_p}{G}\left(\frac{h}{a}\right)^3, \quad \lambda_1 = \frac{32\pi(1-\nu)}{3(1-\nu_p)} \tag{30}$$

From thermodynamic considerations for positive definite strain energy in both the elastic medium and the elastic diaphragm [33], we require $\lambda_1 \in 16(1,4)/9$. The compressive contact pressure distribution on the diaphragm is given by

$$\frac{\sigma_{zz}(r,0)}{p_0} = 1 - \frac{\pi}{(6\kappa + \Omega\lambda_1)}\left[\frac{8}{3}\,{}_2F_1\left(-\frac{3}{2},\frac{3}{2};2;\frac{r^2}{a^2}\right) - 3\left(\frac{r^2}{a^2}\right)\,{}_2F_1\left(-\frac{1}{2},\frac{5}{2};3;\frac{r^2}{a^2}\right)\right] \tag{31}$$

The procedures described in the previous sections can be extended to include other variations in the deflected shape of the diaphragm. As an example, we consider the problem where the deflected shape of the diaphragm can be expressed in the form

$$w(r) = -\frac{C_0^*}{a}[a^2 - r^2] \tag{32}$$

and illustrated in Figure 3. This assumed form of the deflected shape will satisfy the kinematic constraints

$$w(a) = \left[\frac{\mathrm{d}w}{\mathrm{d}r}\right]_{r=0} = 0 \tag{33}$$

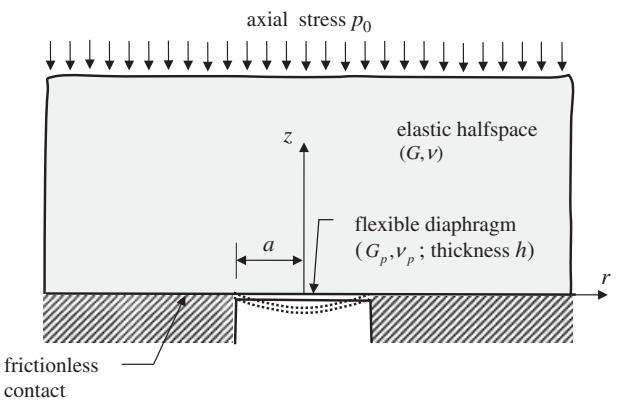

Figure 3. Geometry of the diaphragm for the contact problem. Deflected shape defined by (32).

DOI: 10.1002/nag

which will allow a rotation of the diaphragm and gives rise to a flexural moment at the edge $r = a$. For the purposes of application of the variational principle it is only necessary and sufficient that the deflected shape be kinematically admissible. It must be pointed out that, from the point of view of the engineering design of the diaphragm, it will not be realistically possible to have a *hermetically sealed sensor* that will allow rotations of the diaphragm at its boundary. This example is provided only for the purpose of illustrating the versatility of the variational procedure. The procedure for obtaining the variational solution corresponding to the assumed form of the deflection (32) is identical to that described previously. The total potential energy function can be evaluated in the form

$$U = \frac{\mu a^3 G(C_0^*)^2}{(1-\nu)} + 4\pi D(1+\nu_p)(C_0^*)^2 - \frac{\pi p_0 C_0^* a^3}{2} \tag{34}$$

where $\mu = \frac{16}{15}$. Omitting details of the calculations, it can be shown that the deflection of the diaphragm can be expressed in the form

$$w(r) = \frac{\pi p_0 a(1-\nu)}{G(4\mu + \Omega\lambda_2)}\left(1 - \frac{r^2}{a^2}\right) \tag{35}$$

where

$$\lambda_2 = \frac{8\pi}{3}\frac{(1+\nu_p)(1-\nu)}{(1-\nu_p)} \tag{36}$$

and, from thermodynamic considerations, $\lambda_2 \in 4\pi(1,6)/3$. Similarly, the compressive contact stress distribution on the diaphragm is given by

$$\frac{\sigma_{zz}(r,0)}{p_0} = 1 - \frac{\pi}{(4\mu + \Omega\lambda_2)}\left[2{}_2F_1\left(-\frac{1}{2},\frac{3}{4};2;\frac{r^2}{a^2}\right) - \frac{3}{4}\left(\frac{r^2}{a^2}\right)\ {}_2F_1\left(-\frac{1}{2},\frac{5}{2};3;\frac{r^2}{a^2}\right)\right] \tag{37}$$

3. LIMITING CASES AND NUMERICAL RESULTS

Since the variational estimates for the deflections of the diaphragm can be evaluated in *exact closed forms*, it is not necessary to give extensive numerical results, particularly for the deflected shapes and for the flexural stresses at the centre of the diaphragm, which are used for the interpretation of the applied stress state p_0. In the limiting case as the stiffness of the diaphragm becomes large or as $D \to \infty$, the diaphragm deflection $w(r)$ reduces to zero and the contact pressure at the elastic solid–rigid diaphragm interface is the applied stress p_0. As indicated previously, the limit of $D \to 0$ is excluded in the first analysis by virtue of the assumed form of the deflected shape for the diaphragm (6), that maintains a zero slope at the diaphragm boundary $r = a$. In the event $D \to 0$, the problem reduces to that of an elastic solid that is compressed against a rigid boundary with an opening of radius a. The resulting mixed boundary value problem is mathematically identical to the problem of the tensile loading of a half domain of a penny-shaped crack located in an elastic solid of infinite extent, and defined by the mixed boundary value problem given in (11)–(13). In this case the deflection of the elastic solid takes the form

$$u_z(r,0) = \frac{2(1-\nu)p_0 a}{\pi G}\left(1 - \frac{r^2}{a^2}\right)^{1/2} \tag{38}$$

DOI: 10.1002/nag

whereas the appropriate reduction of (29) gives

$$u_z(r,0) = \frac{2(1-v)p_0 a}{\pi G}\left(\frac{\pi^2}{12\kappa}\right)\left(1-\frac{r^2}{a^2}\right)^2 \tag{39}$$

If deflections of the contacting elastic medium are measured at the centre opening to interpret the contact pressure field, then in the worst case, the variational result corresponding to the assumed deflected shape given by (29) will under-predict the pressure by approximately 14%. Similarly, the appropriate reduction of (35) as $D \to 0$ gives

$$u_z(r,0) = \frac{2(1-v)p_0 a}{\pi G}\left(\frac{\pi^2}{8\mu}\right)\left(1-\frac{r^2}{a^2}\right) \tag{40}$$

and the assumed deflected shape will be under-predicted by approximately 16%. When the flexural stiffness of the diaphragm is set to zero, the strain in the diaphragm is not an appropriate indicator for interpreting the contact pressure. Such a flexible diaphragm will, of course, entirely invalidate the purpose of providing a sensor diaphragm that will not act as an anomaly. Contact stress transducers are designed to undergo imperceptible deformations that are within the capabilities of the sensing technique and the sensor readings are used to determine either the deflection or the strains in the diaphragm.

In the case where the flexural rigidity of the diaphragm is finite, the flexural moments at the centre of the diaphragm can be used to interpret the contact pressure. For the deflection of the diaphragm prescribed by (29), the maximum flexural moment, which can be used to interpret the measured contact pressures through the measured strains, is given by

$$M_{rr}(0) = M_{\theta\theta}(0) = \frac{2\pi D p_0(1-v)(1+v_p)}{Ga(6\kappa+\Omega\lambda_1)} \tag{41}$$

Similarly, the maximum flexural moment corresponding to the deflected shape (35) is given by

$$M_{rr}(0) = M_{\theta\theta}(0) = \frac{2\pi D p_0(1-v)(1-v_p)}{Ga(4\mu+\Omega\lambda_2)} \tag{42}$$

Figure 4 presents, for purposes of illustration, the variation of contact pressures at the diaphragm–elastic medium interface for specific choices of the relative stiffness parameter Ω for the case where the diaphragm deflections are defined by (29) and $\lambda_1 = \frac{32}{9}$. Figure 5 illustrates similar results for the case where the deflection of the diaphragm are denoted by (35) and $\lambda_2 = 4\pi$. These results indicate that for a relatively flexible diaphragm, arching action can develop and the stresses are borne primarily by the boundary regions of the flexible diaphragm. Figures 6 and 7 illustrate the variation in the contact pressure at the centre of the flexible diaphragm as a function of the relative stiffness parameter Ω and the extreme values of λ_1 and λ_2, respectively. These results illustrate the relative limiting values of Ω needed to achieve a contact pressure consistent with that applied at the surface of the elastic medium.

The validity of the variational approach presented in the paper ultimately depends on the accuracy of the displacement functions for the flexible diaphragm in representing plausible deflected shapes for a range of relative rigidity parameters. This can only be tested through an analysis of the complete diaphragm–elastic halfspace interaction problem in which no *a priori* restrictions are placed on the form of the deflected shape. For purposes of comparison, we develop here a finite element estimate of the analysis of the interaction problem. The finite element code ABAQUS^{TM} is used to examine the axisymmetric problem where the elastic

DOI: 10.1002/nag

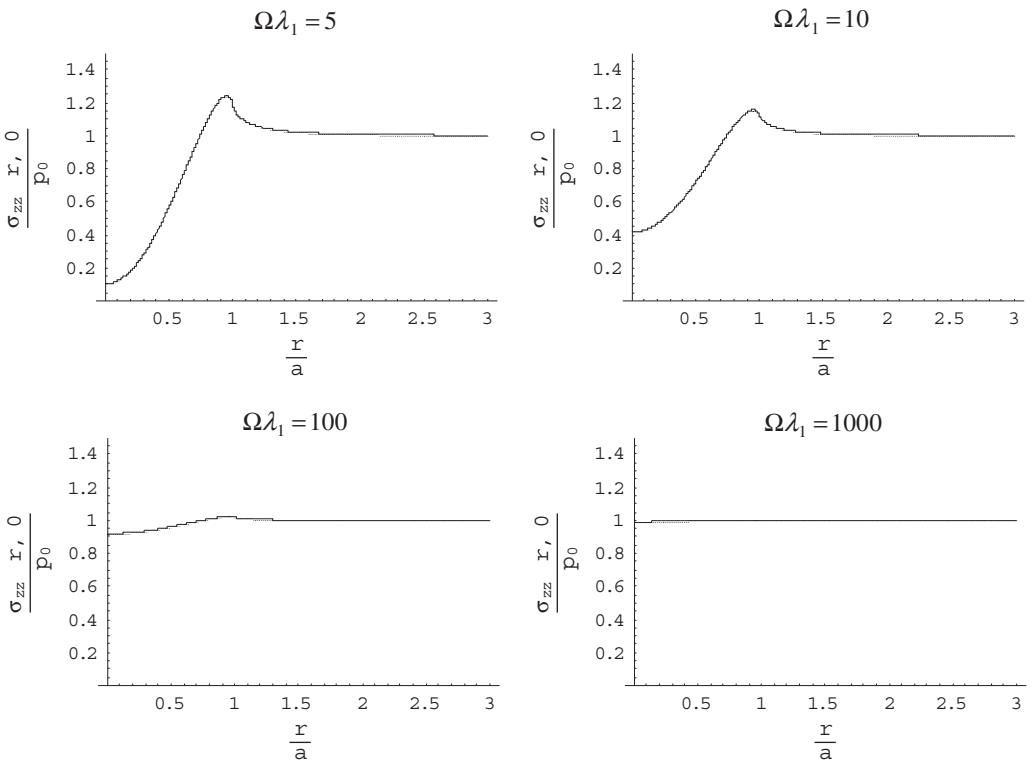

Figure 4. Influence of the relative stiffness on the contact pressure distributions at the diaphragm–elastic medium interface. [Deflections of the flexible diaphragm defined by (29).]

medium and the elastic diaphragm are modelled, respectively, by 8-noded serendipity isoparametric elements and bi-quadratic axisymmetric quadrilaterals with two degrees of freedom. Each contain two active degrees of freedom and reduced integration (CAX8R) is used throughout. In this computational treatment, no attempt is made to incorporate infinite elements to model the halfspace region that is in smooth contact with the flexible diaphragm. Instead, the influence of the finite extent of the domain is examined by considering regions where (i) the plane surface of the elastic medium, which is subjected to the uniform stress p_0, is located at a distance of $10a$ from the elastic diaphragm, where a is the radius of the diaphragm and either (ii) the outer boundary of the elastic layer region is located at a radius of $20a$ and smoothly constrained (Figure 8) or (iii) the outer boundary of the elastic layer is located at a radius of $30a$ and maintained traction free (Figure 9). The finite element discretizations of the diaphragm–elastic medium system are also shown in Figures 8 and 9. The conditions at the boundary of the diaphragm can vary between complete fixity and zero slope at the boundary $r = a$ to only continuity of displacements at the same boundary. Suitable mesh refinement of the elastic layer region is employed at the boundary $r = a$ to ensure that the sharp stress gradients that can occur at the boundary are adequately evaluated. Again, there is no provision to incorporate singularity elements at the boundary of the diaphragm. The *arbitrarily chosen*

DOI: 10.1002/nag

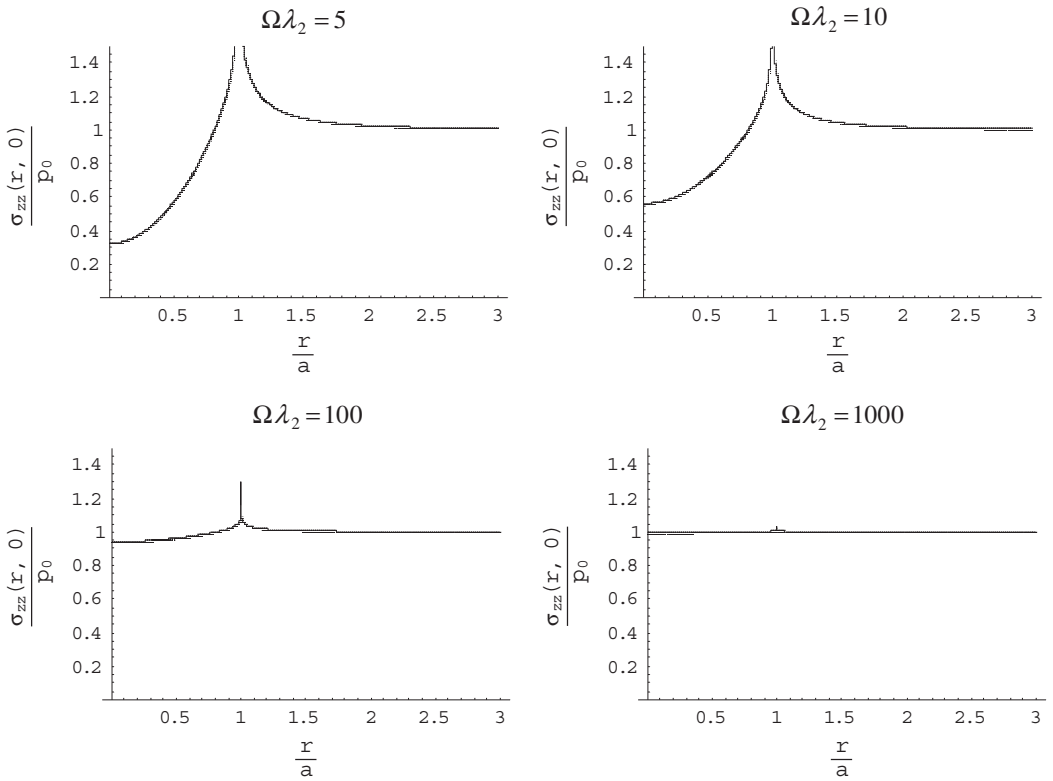

Figure 5. Influence of the relative stiffness on the contact pressure distributions at the diaphragm–elastic medium interface. [Deflections of the flexible diaphragm defined by (35).]

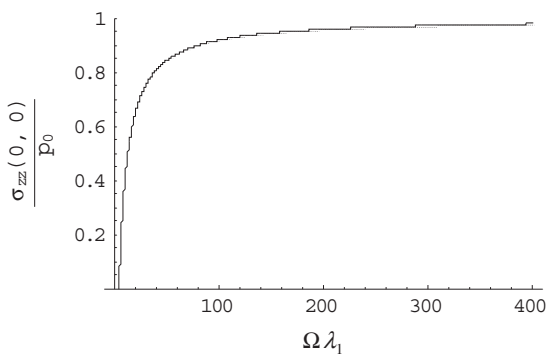

Figure 6. Influence of the relative stiffness parameter $\Omega\lambda_1$ on the contact pressure distributions at the centre of the flexible diaphragm. [Deflections of the flexible diaphragm defined by (29).]

elasticity parameters for the elastic halfspace region are assigned the following values: $G = 5.2$ MPa and $\nu = \frac{1}{3}$. The elastic constants for the material forming the flexible diaphragm are $G_p = 80$ GPa and $\nu_p = \frac{1}{4}$. The dimensions of the diaphragm are as follows: diaphragm

DOI: 10.1002/nag

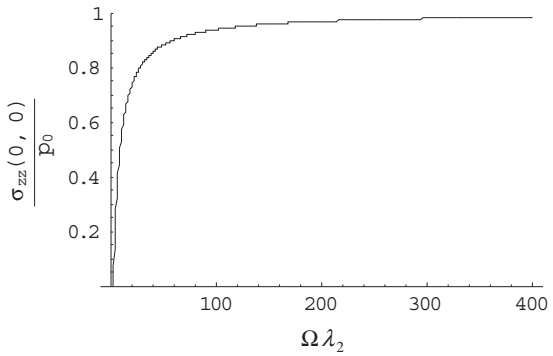

Figure 7. Influence of the relative stiffness $\Omega\lambda_2$ on the contact pressure distributions at the centre of the flexible diaphragm. [Deflections of the flexible diaphragm defined by (35).]

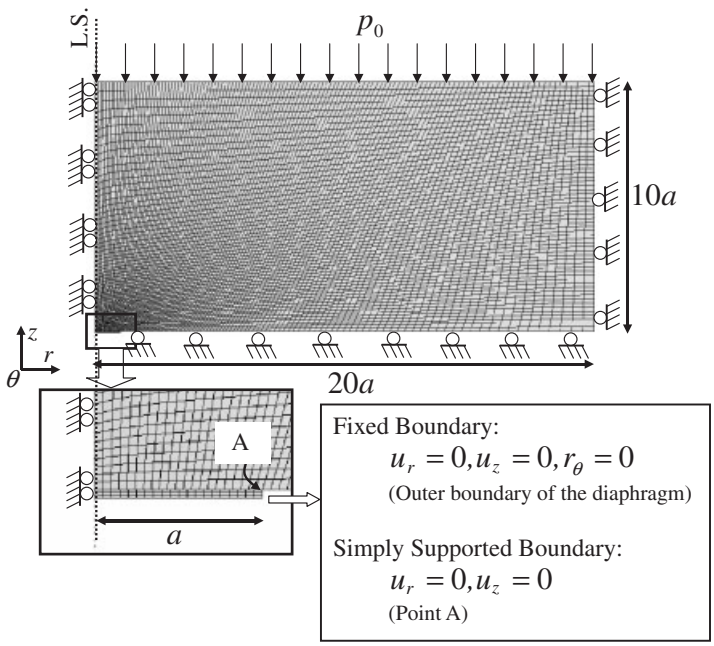

Figure 8. Finite element discretization of the axisymmetric problem involving the interaction between a plate element and an elastic layer of finite extent. (Case 1: smoothly constrained outer boundary; 6975 elements in the elastic layer and 60 elements in the diaphragm.)

thickness $h = 0.5$ mm and diaphragm radius $a = 10$ mm. The elastic layer region is subjected to a uniform surface stress of $p_0 = 100$ kPa.

Figure 10 illustrates the comparison between the results for the deflections of the diaphragm as obtained from the variational procedure and those derived from the computational approach for the case where the boundary of the flexible diaphragm exhibits fixity. There is excellent

DOI: 10.1002/nag

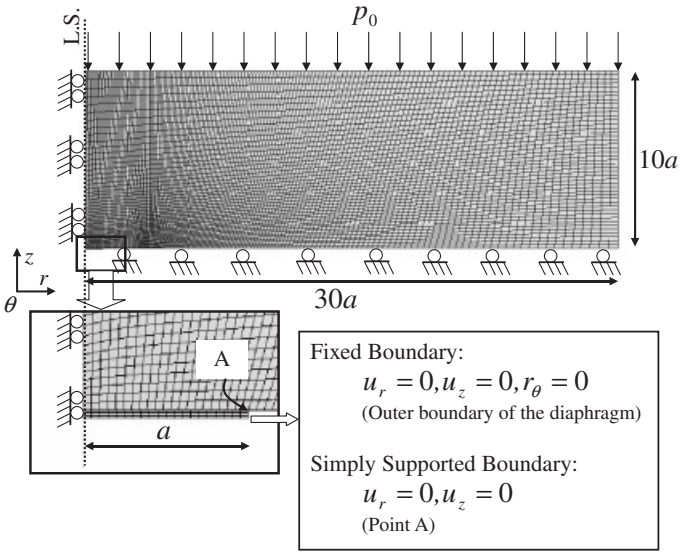

Figure 9. Finite element discretization of the axisymmetric problem involving the interaction between a plate element and an elastic layer of finite extent. (Case 2: traction-free outer boundary; 7500 elements in the elastic layer and 60 elements in the diaphragm.)

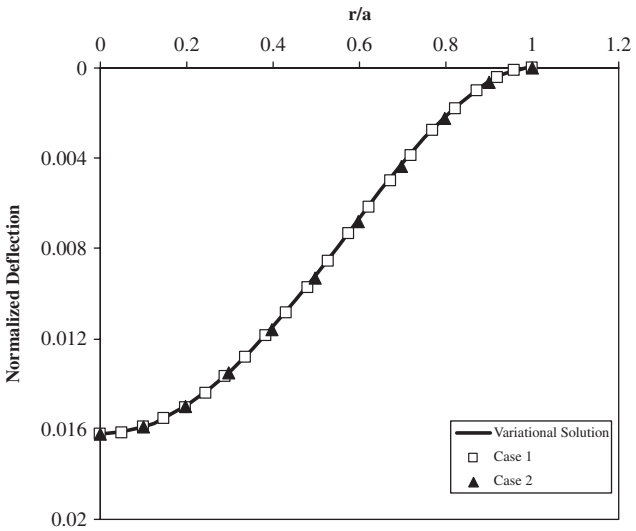

Figure 10. Comparison of results for the deflection of the flexible diaphragm with fixity at the diaphragm boundary. (Case 1 refers to the results obtained with the finite element model where the boundary of the elastic domain is smoothly constrained; Case 2 refers to the results obtained with the finite element model where the outer boundary is traction free.) [The normalized diaphragm deflection is given by $w(r)G/\pi p_0 a(1-\nu)$.]

DOI: 10.1002/nag

agreement between the separate sets of results. Figure 11 illustrates the distribution of contact normal stresses at the interface between the elastic medium and the rigid boundary with the flexible diaphragm for the case where the boundary of the flexible diaphragm exhibits fixity. Again, there is excellent agreement between the variational solution and the computational results both in terms of the magnitude and distribution of the normalized contact normal stress. It is also important to note that, as required from *Saint-Venant's principle* applicable to elastic systems [3, 26], the contact normal stresses reduce to the value p_0 at radial distances remote from the flexible diaphragm. In effect, the influences of the flexible diaphragm in perturbing the uniform stress state at the rigid boundary are felt only within a radius of $r<4a$. Figure 12 illustrates the comparison between the results for the deflections of the diaphragm as obtained from the variational procedure and those derived from the computational approach for the case where there is only continuity of displacements at the boundary of the flexible diaphragm. In this case there is a substantial discrepancy between the results obtained from the variational approach and the computational results. The accuracy of the variational estimate can be improved by selecting a displacement function that satisfies both the kinematic constraints (33) and gives zero flexural moments in the radial direction. Since this solution is given only for purposes of comparison, such a detailed treatment is unwarranted. Figure 13 illustrates the distribution of contact normal stresses at the interface between the elastic medium and the rigid boundary with the flexible diaphragm for the case where the displacements of the boundary are zero. In this case, the trends indicated by the various solutions are consistent, although the numerical values differ due to the absence of a computational procedure to account for singularities in the stress field at the boundary of the flexible diaphragm.

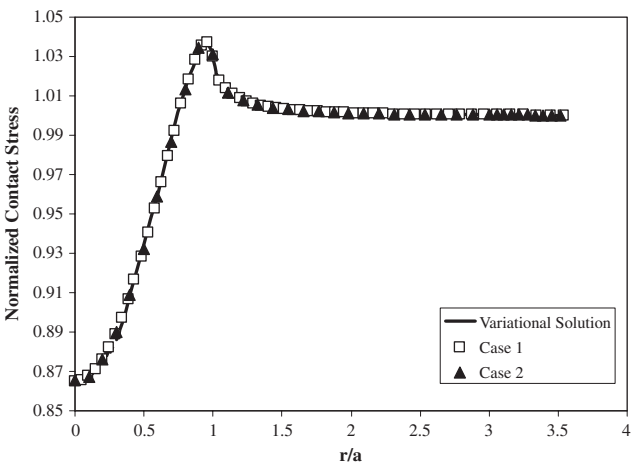

Figure 11. Comparison of results for the contact normal stresses at the flexible diaphragm–elastic medium interface with fixity at the boundary. (Case 1 refers to the results obtained with the finite element model where the boundary of the elastic domain is smoothly constrained; Case 2 refers to the results obtained with the finite element model where the outer boundary is traction free.) [The normalized contact stress is given by $\sigma_{zz}(r,0)/p_0$.]

DOI: 10.1002/nag

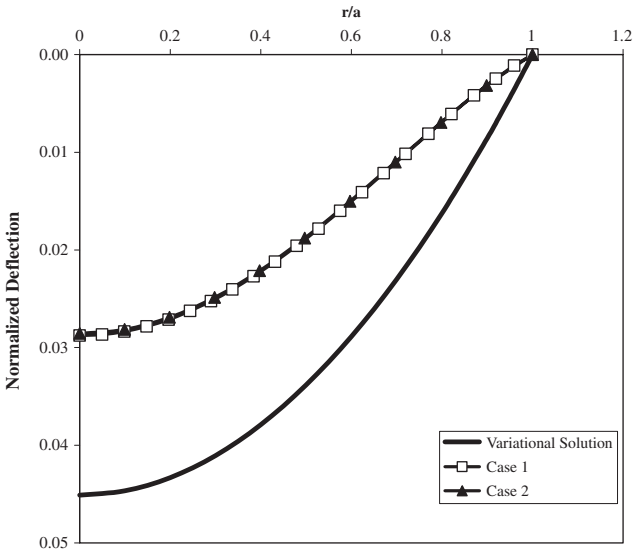

Figure 12. Comparison of results for the deflection of the flexible diaphragm with displacement continuity at the diaphragm boundary. (Case 1 refers to the results obtained with the finite element model where the boundary of the elastic domain is smoothly constrained; Case 2 refers to the results obtained with the finite element model where the outer boundary is traction free.) [The normalized diaphragm deflection is given by $w(r)G/\pi p_0 a(1-\nu)$.]

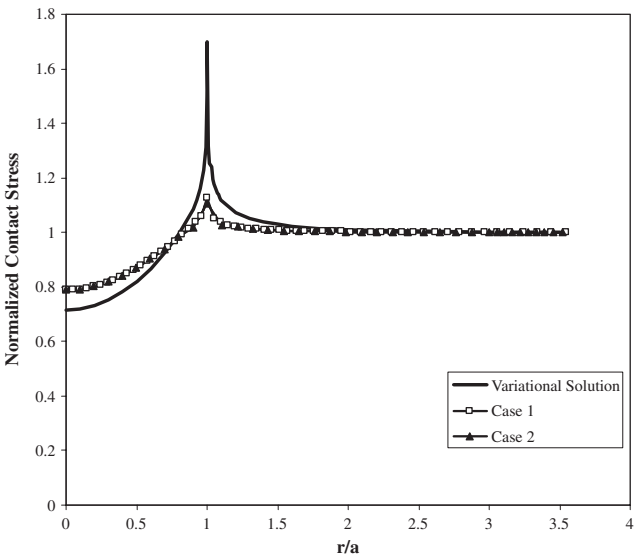

Figure 13. Comparison of results for the contact normal stresses at the flexible diaphragm–elastic medium interface with displacement continuity at the diaphragm boundary. (Case 1 refers to the results obtained with the finite element model where the boundary of the elastic domain is smoothly constrained; Case 2 refers to the results obtained with the finite element model where the outer boundary is traction free.) [The normalized contact stress is given by $\sigma_{zz}(r,0)/p_0$.]

DOI: 10.1002/nag

4. CONCLUDING REMARKS

This paper illustrates the application of a variational technique for modelling the interaction of a flexible diaphragm with an elastic region of semi-infinite extent. The smooth contact between the regions ensures that the far-field stresses are normal to the plane boundary. This is an idealization that presents a limiting case of an actual contact surface that can possess either Coulomb friction or finite friction. The complete formulation of the interaction problem will require the solution of an integro-differential equation governing the elastostatic contact problem. The integro-differential nature of the title problem results from the coupling of the thin plate flexure with the mixed boundary value problem for a halfspace. This approach invariably requires recourse to numerical techniques. This paper presents an alternative approach that is based on a classical variational technique. The success of a variational technique ultimately depends on the choice of the kinematically admissible functions used to represent the deflection of the diaphragm. The choice of the fourth-order polynomial explicitly satisfies the boundary conditions applicable to the flexure of a diaphragm that is fixed at the periphery. This implies that the solution developed *via* the variational scheme is valid for most situations where the relative stiffness parameters $\Omega\lambda_i$, $(i = 1, 2)$, for the diaphragm–elastic medium system are large. This would indeed be the case in most situations involving pressure-sensing devises. The choice of the second-order polynomial satisfies continuity of displacements but not its derivative. This invariably introduces a singular stress state at the boundary of the flexible diaphragm region. The analysis of the associated variational problems is facilitated through the use of solutions applicable to mixed boundary value problems in elasticity together with the theory of Abel integral equations. The analyses provide convenient results that relate either the central deflection of the circular diaphragm or the flexural moments at the centre to the applied contact stress, through a relative stiffness parameter that incorporates the elasticity parameters of both materials and the geometric parameters of the circular diaphragm. The results for the case where the deflected profile of the flexible diaphragm has only displacement continuity is presented for purposes of comparison. This can also be regarded as a limiting case where the flexibility of the diaphragm would allow the development of a non-zero slope at the boundary without initiating plastic or irreversible deformations of the diaphragm. Variational solutions of the type described provide convenient first approximations for preliminary calculation of pressure sensor performance. To assess the reliability of the variational approximation, the solutions derived from the analytical scheme are also compared with results derived from a finite element model of the diaphragm–elastic medium interaction problem, for a set of arbitrarily chosen material and geometric parameters. The results from the finite element analysis indicate the same trends and magnitudes in the displacements and contact pressure distributions as observed in the variational solutions, for the case where the boundary of the flexible diaphragm exhibits fixity. The results further illustrate the efficiency and economy of the analytical method [34, 35] in providing compact solutions to problems of importance to geotechnical engineering and geomechanics.

The contact pressure distribution at the diaphragm–elastic medium interface is a useful indicator for assessing the influence of the diaphragm flexibility on the reliability of measurements derived from the contact pressure transducer, since the strains measured at the centre of the diaphragm region are influenced by the contact pressure distribution. It is also clear that, regardless of the nature of the fixity conditions at the boundary, the accuracy of the

DOI: 10.1002/nag

measured stress increases as the relative stiffness parameter $\Omega\lambda_i$ increases. This observation can be used to determine the basic geometry of the sensor region that optimizes the deflections and strains in the diaphragm to provide the desired accuracy. It also reinforces the point that calibrations of contact pressure cells and transducers using fluids under pressure has no value and will invariably give rise to erroneous interpretations of the measured contact pressure. The boundary pressure cell is a particularly simple case and, in instances where the cell is located within a deformable medium, the '*inclusion factor*' can have an added influence on the interpretation of the stress state remote from the cell. In the instance where the constitutive response of the medium in contact with the diaphragm has a complicated non-linear form applicable to geomaterials that exhibit either non-linear phenomena in the small strain range, or have a granular internal structure, and when contact friction is involved, recourse must invariably be made to computational methodologies to establish the mechanics of the interaction. In these situations, the measured contact pressures can also depend on the stress history associated with the loading paths followed by the externally applied pressures. An example of experimental results derived from loading–unloading response of the measured pressures by a pressure transducer located at a rigid boundary and in contact with a granular material is shown in Figure 14. The explanation of the strong path dependency in the observed response requires the use of computational methods and appropriate constitutive models of granular material behaviour for the study of the elastic diaphragm–geomaterial interaction. These investigations are relegated to future studies.

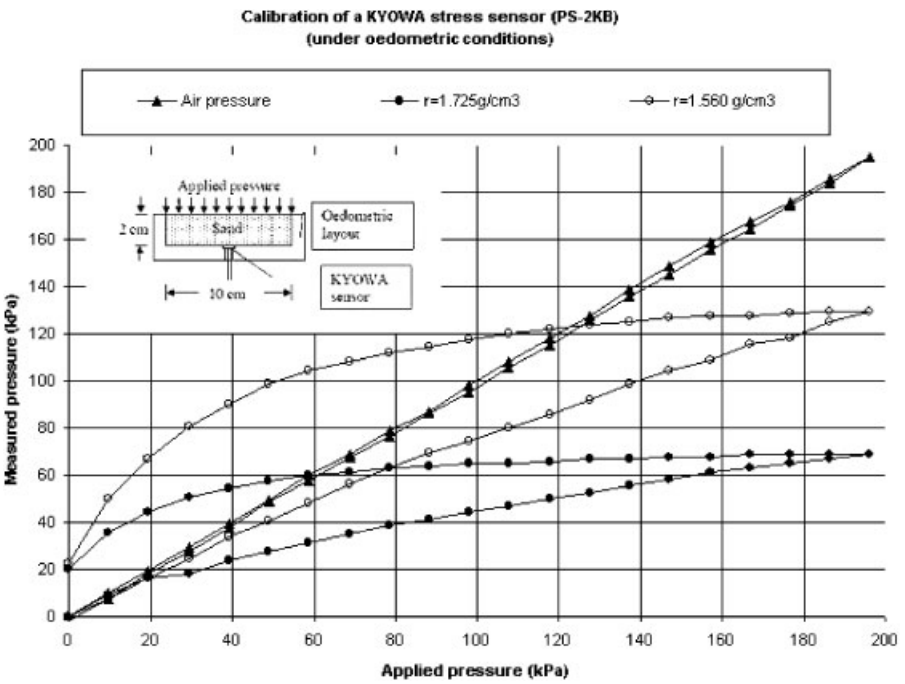

Figure 14. Role of material non-linearities and loading history on the contact pressures inferred from measurements conducted with a diaphragm-type pressure transducer.

DOI: 10.1002/nag

ACKNOWLEDGEMENTS

One of the authors (APSS) would like to thank the Laboratoire 3S, Université Joseph Fourier and INPG-ENSHMG, Grenoble, France, for a Visiting Professor appointment in 2006, during the tenure of which this paper was completed. The support provided to the first author through the *Max Planck Forschungspreis in the Engineering Sciences*, awarded by the Max Planck Gesellschaft, Germany is also gratefully acknowledged. The authors are grateful to Mr H. Ghiabi for assistance with the finite element computations.

REFERENCES

1. Hast N. *Measuring Stresses and Deformations in Soil Materials*. Ingenjörsvetenskapsakad, Handl. No. 178, Stockholm, Sweden, 1945.
2. Hvorslev MJ. The changeable interaction between soils and pressure cells: tests and reviews at the waterways experiment station. *Technical Report No. 5-76-7*, U.S. Army Corps of Engineers, Waterways Experiment Station, Vicksburg, MI, 1976.
3. Selvadurai APS. *Elastic Analysis of Soil–Foundation Interaction. Developments in Geotechnical Engineering*, vol. 17. Elsevier Scientific Publ. Co.: Amsterdam, 1979.
4. Kulhawy FH (ed.). Recent developments in geotechnical engineering for hydro-projects: embankment dam instrumentation and performance, engineering geology aspects, rock mechanics studies. *Proceedings of the International Conference*. ASCE: New York, 1981.
5. Hanna TH. *Field Instrumentation in Geotechnical Engineering*. Trans-Tech. Publ.: Clausthal-Zellerfeld, 1985.
6. Dunnicliffe J, Green GE. *Geotechnical Instrumentation for Monitoring Field Performance*. Wiley-Interscience: New York, 1988.
7. Sinha RS. *Underground Structures*; *Design and Instrumentation*, *Developments in Geotechnical Engineering*, vol. 59a. Elsevier Scientific Publ. Co.: Amsterdam, 1989.
8. Lazebnik GE. *Monitoring of Soil–Structure Interaction*. Chapman & Hall: London, 1998.
9. Webster JG. *Tactile Sensors for Robotics and Medicine*. Wiley: New York, 1988.
10. Tandeske D. *Pressure Sensors*: *Selection and Application*. Marcel Dekker: New York, 1991.
11. Bao M-H. *Micro-Mechanical Transducers*, *Pressure Sensors*, *Accelerometers and Gyroscopes*. Elsevier Scientific Publ. Co.: Amsterdam, 2000.
12. Mak AFT, Zhang M, Boone DA. State-of-the-art research in lower-limb prosthetic biomechanics-socket interface: a review. *Journal of Rehabilitation Research and Development* 2001; **38**:161–174.
13. Gohar R. *Elastohydrodynamics*. Imperial College Press: London, 2001.
14. Gad-el-Hak M. *The MEMS Handbook*. CRC Press: Boca Raton, FL, 2002.
15. Boyes W (ed.). *Instrumentation Reference Book*. Butterworth-Heinemann: Boston, 2003.
16. Beeby S. *MEMS Mechanical Sensors*. Arctec House: Boston, 2004.
17. Nawrocki W. *Measurement Systems and Sensors*. Arctec House: Boston, 2005.
18. Dunn WC. *Introduction to Instrumentation*, *Sensors and Process Control*. Arctec House: Norwood, 2006.
19. Lewis G. Contact stress at articular surfaces in total joint replacements. Part 1. Experimental methods. *Bio-medical Materials and Engineering* 1998; **8**:91–110.
20. Lewis G. Contact stresses at articular surfaces in total joint replacements. Part II. Analytical and numerical methods. *Bio-medical Materials and Engineering* 1998; **8**:259–278.
21. Labanieh S, Elhajal J. Reliability of stress measurements in geomechanics. In *Proceedings of the 3rd International Symposium on Field Measurements in Geomechanics*, Sørum G, Oslo AA (eds). Balkema: Rotterdam, 1991; 153–158.
22. Selvadurai APS. An energy estimate of the flexural deflections of a circular foundation embedded in an elastic medium. *International Journal for Numerical and Analytical Methods in Geomechanics* 1979; **3**:285–292.
23. Selvadurai APS. Elastic contact between a flexible circular plate and a transversely isotropic elastic halfspace. *International Journal of Solids and Structures* 1980; **16**:167–176.
24. Selvadurai APS. A contact problem for a Reissner plate and an isotropic elastic halfspace. *Journal of Theoretical and Applied Mechanics* 1984; **3**:181–196.
25. Timoshenko SP, Woinowsky-Krieger S. *Theory of Plates and Shells*. McGraw-Hill: New York, 1959.
26. Selvadurai APS. *Partial Differential Equations in Mechanics*, *Vol. 2. The Biharmonic Equation*, *Poisson's Equation*. Springer: Berlin, 2000.
27. Sneddon IN. The distribution of stress in the neighbourhood of a crack in an elastic solid. *Proceedings of the Royal Society*, *Series A* 1946; **18**:229–260.
28. Sneddon IN (ed.). *Application of Integral Transforms in the Theory of Elasticity*. Springer: Wien, 1975.
29. Love AEH. *A Treatise on the Mathematical Theory of Elasticity*. Dover: New York, 1944.

DOI: 10.1002/nag

30. Green AE. On Boussinesq's problem and penny-shaped cracks. *Proceedings Cambridge Philosophical Society* 1949; **45**:251–257.
31. Gorenflo R, Vessella S. *Abel Integral Equations. Analysis and Applications*. Lecture Notes in Mathematics, vol. 1461. Springer: Berlin, 1991.
32. Abramowitz M, Stegun I. *Handbook of Mathematical Functions*. Dover: New York, 1972.
33. Davis RO, Selvadurai APS. *Elasticity and Geomechanics*. Cambridge University Press: Cambridge, 1996.
34. Gibson RE. The analytical method in soil mechanics. *Geotechnique* 1974; **24**:115–140.
35. Selvadurai APS. The analytical method in geomechanics. *Applied Mechanics Reviews* 2007, in press.

DOI: 10.1002/nag